A Hybrid Feedback Control Strategy for Autonomous Waypoint Transitioning and Loitering of Unmanned Aerial Vehicles

Dean W. Smith III[a], Ricardo G. Sanfelice[b]

[a] *Guidance Navigation and Control Center. Raytheon Missile Systems, Tucson, AZ*
[b] *Computer Engineering Department. University of California, Santa Cruz, CA*

Abstract

We consider the problem of autonomously controlling a fixed-wing aerial vehicle to visit a neighborhood of a pre-defined waypoint, and when nearby it, loiter around it. To solve this problem, we propose a hybrid feedback control strategy that unites two state-feedback controllers: a *global controller* capable of steering or transitioning the vehicle to nearby the waypoint and a *local controller* capable of steering the vehicle about a loitering radius. The aerial vehicle is modeled on a level flight plane with system performance characterized in terms of the aerodynamic, propulsion, and mass properties. Thrust and bank angle are the control inputs. Asymptotic stability properties of the individual control algorithms, which are designed using backstepping, as well as of the closed-loop system, which includes a hybrid algorithm uniting the two controllers, are established. In particular, for this application of hybrid feedback control, Lyapunov functions and hybrid systems theory are employed to establish stability properties of the set of points defining loitering. The analytical results are confirmed numerically by simulations.

1. Introduction

1.1. Background

Autonomous navigation of unmanned aerial vehicles (UAVs) requires algorithms that are capable of accurately controlling the motion of the vehicle with only limited control authority. Such algorithms should be capable of precisely controlling the position, orientation, and velocity of the vehicle by properly generating forces and torques through thrusters, propellers, moving surfaces, etc. A wide range of tasks for such vehicles can be recast as the problem of steering the vehicle to a path given by closed curve, e.g., a straight line or a loitering pattern. To accomplish such tasks, control algorithms capable of maintaining the vehicle aloft along the given path are required. Recent results in the literature demonstrate that feedback control algorithms can be designed to steer UAVs along different paths by "reshaping" the vector fields that describe the motion of the vehicle under the effect of a guidance law defined by a particular

set of differential equations [1, 2]. The authors of [2] argue that their reshaping approach is explicit (in the sense that the task to accomplish is pre-defined) and that avoids potential complications of trajectory planning and tracking. While performance is not assessed in [2], the performance of tracking control algorithms given in terms of linear, static state-feedback laws deteriorates when curved paths are to be tracked. A study of performance of tracking algorithms was reported in [3], where a nonlinear guidance logic for trajectory tracking of UAVs that overcomes the inherent limitation of linear feedback control in following curved paths is proposed.

An alternative to the vector field shaping technique mentioned above is to rely on multiple controllers, each of them designed to accomplish a different task, and appropriately switch among them. In such approach, a supervisory control algorithm monitors the state of the vehicle and, based on the given mission, determines which controller should be applied at each instant. The switching logic should be capable of "piecing together" the individual controllers to achieve the desired vehicle motion while precluding chattering around the set of points defining the switching condition. While the approach allows independent design of the individual controllers, the emergence of discrete (or discontinuous) dynamics is unavoidable, which may make the analysis more involved (e.g., see the example in [4], which shows that two controllers – a local and a global continuous-time controller – cannot be united using a continuous-time supervisor). Furthermore, the condition triggering the switches between the controllers has to involve memory so as to avoid chattering [5].

Fortunately, recent advances in the literature of hybrid systems have made systematic design of control algorithms piecing together individual controllers possible [6]. Interestingly, the design of such systems can be performed to yield a closed-loop system that not only is chattering-free but also is robust with respect to measurement noise, actuator errors, and external disturbances; see, e.g., [7]. Due to these unique capabilities, the said hybrid systems approach to the combination of multiple controllers has been successfully employed in different applications, such as the stabilization of an inverted pendulum [6] and of the position and orientation of a mobile robot [8]. Furthermore, the technique has been extended in [9] to allow for the combination of multi-objective controllers, including state-feedback laws as well as open-loop control laws. In the context of performance, a trajectory-based approach was also employed in [10] to generate dwell-time and hysteresis-based control strategies that guarantee an input-output stability property characterizing closed-loop system performance. More related to the application studied in this paper, algorithms for vehicles that use multiple controllers coordinated by a supervisory algorithm also lead to a hybrid system and have been proposed in the literature. A review of such works and an algorithm for the control of single and multiple UAVs appeared in [11], where a hybrid automaton with modes corresponding to each control task is proposed and an example of an altitude hybrid controller for a fixed wing UAV is presented. A general formulation of the motion planning problem for dynamical systems with symmetries, which, in particular, includes models of vehicles, appeared in [12], where a general language for trajectory genera-

tion using motion primitives; see also the robustification via supervisory hybrid feedback control [13].

1.2. Contributions

In this paper, we employ the hybrid approach outlined above to provide a solution to the problem of autonomously controlling a fixed wing aerial vehicle to visit a neighborhood of a pre-defined waypoint, and when nearby it, loiter around it without chattering. More precisely, we propose a hybrid feedback control strategy that unites two state-feedback controllers: a *global controller* capable of steering or transitioning the vehicle to nearby the waypoint and a *local controller* capable of steering the vehicle about a loitering radius. Following [14], the aerial vehicle is modeled on a level flight plane with system performance characterized in terms of the aerodynamic, propulsion, and mass properties. The resulting model is nonlinear and with thrust and bank angle being its control inputs. This nonlinear UAV bank-to-turn model partially resembles a ship course controller model [15], where heading is controlled indirectly through the heading rate. For this vehicle model and employing Lyapunov stability theory, we establish key asymptotic stability properties of the individual control algorithms designed. Both the local and global controllers are designed using the backstepping control design technique [16, 17]. With the region of attraction induced by each controller being characterized, the closed-loop system incorporating a hybrid algorithm uniting the individual controllers is shown to be asymptotically stable using stability tools for hybrid dynamical systems. We are not aware of a similar solution for this UAV problem, for which the application of hybrid systems theory leads to a hybrid feedback control algorithm that is chattering-free and with rigorously established properties of the region of attraction.

1.3. Organization of the paper

The remainder of the paper is organized as follows. Section 2 formulates the problem to solve, introduces the model of the vehicle, and proposes the structure of the hybrid controller to be designed. The main results follow in Section 3. This section starts by recasting the problem of interest as a set stabilization problem. Then, it provides the design of the local and global controllers in two steps: first, a controller when actuation is through thrust and heading angle (Section 3.1) and, second, using backstepping, a controller when the actuation is through thrust and bank angle (Section 3.2). In Section 3.3, a hybrid controller combining the two previously designed controllers and the properties it confers to the closed-loop system are presented. In Section 4, the proposed control law and the results are validated in several simulations.

1.4. Notation and Nomenclature

$\|x\|$	Euclidean norm of x
$\mathcal{A}$	Set to be stabilized
c	level set, constant
$\mathcal{C}$	Hybrid system flow set
C_D	Drag coefficient
C_{D0}	Zero lift drag coefficient
C_L	Lift coefficient
$\mathcal{D}$	Hybrid system jump set
D	Drag, N
e	Error function
f	Hybrid system flow map
G	Hybrid system jump map
g	Gravity, m/s^2
h	Altitude, m
$\mathcal{H}$	Hybrid system
k	Controller gain
K	Drag Polar Coefficient
$\mathcal{K}_\infty$	Family of continuous functions that are zero at zero, strictly increasing, and unbounded
L	Lift, N
p	Local switching variable
q	Controller index
r	Turn radius, m
R	Magnitude of position vector, m
$\mathbb{R}$	Real numbers
s	dummy variable
S_{ref}	Wing reference area m^2
T	Thrust, N
U	Domain of hybrid system
v	Airspeed, m/s
V	Lyapunov function
W	Weight, N
x	x position, m
y	y position, m
z	State vector of hybrid system
α	class κ_∞ function
κ	Controller
ρ	Air density, kg/m^3
μ	Local controller rotation hysteresis
Ψ	Heading, deg
Φ	Bank angle

Subscripts

0	Initial Condition
b	Body Frame
C	Commanded

2. Problem Formulation

We consider the problem of stabilizing an aerial vehicle to loiter around a given waypoint with specified velocity. Figure 1 depicts the scenario of problem to be solved, where v is the airspeed of the vehicle, $(x, y) \in \mathbb{R}^2$ describe its position, and Ψ its heading angle. In this way, the vehicle's velocity and heading angle are related by

$$v = \sqrt{\dot{x}^2 + \dot{y}^2}, \quad \Psi = \angle \left(\begin{bmatrix} \dot{x} \\ \dot{y} \end{bmatrix} \right), \tag{1}$$

where

$$\angle : \mathbb{R}^2 \setminus \{0\} \rightrightarrows [-\pi, \pi] \tag{2}$$

defines the angle, positive in a clockwise direction, between the vector input and the positive vertical axis (x). Without loss of generality, the waypoint is assumed to be at the origin of the position coordinates (x, y) and the desired radius for loitering is R_C. Note that $\angle$ is undefined when x and y are 0. The forces on the UAV are described in the body frame (x_b, y_b) and can be transformed into the plane of the absolute frame (x, y) using the heading angle Ψ, via

$$\begin{bmatrix} \cos\Psi & -\sin\Psi \\ \sin\Psi & \cos\Psi \end{bmatrix} \tag{3}$$

Several assumptions are made in order to focus the analysis for the scope of this paper. These assumptions are listed below:

- UAV modeled as a point mass;
- Level flight in the (x, y) plane;
- Gravitational acceleration is constant;
- Aerodynamic properties modeled as a simple drag polar with a maximum lift coefficient;
- Propulsion performance is limited by a maximum thrust;
- Mass is constant (no fuel burn);
- Vehicle "banks" to turn and the bank angle Φ satisfies $\Phi \in \left(-\frac{\pi}{2}, \frac{\pi}{2}\right)$.

These assumptions are typical in the conceptual design phase of an aircraft where system level aerodynamic and propulsion performance are balanced to achieve mission objectives.

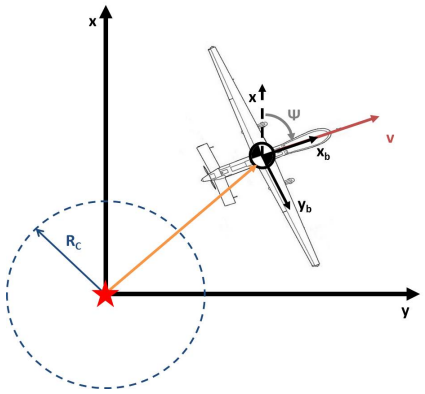

Figure 1: Waypoint Geometry.

2.1. Free Body Diagram

The equations of motion for the UAV are determined by using first principles. The free body diagram for the aircraft is shown in Fig. 2.

Summing the forces in the body axes shown in Fig. 2 gives the equations

$$F_{x_b} = T - D, \tag{4}$$

$$F_{y_b} = L \sin \Phi, \tag{5}$$

$$F_h = W - L \cos \Phi, \tag{6}$$

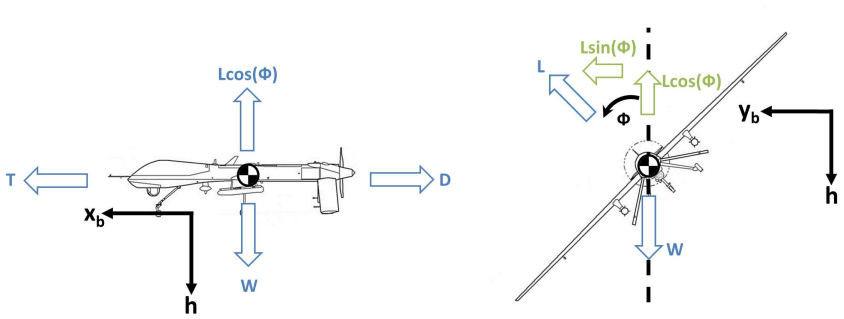

Figure 2: Level Flight Free Body Diagram.

where T is thrust, D is drag , L is lift, W is weight, and Φ is bank angle. Since the problem is simplified to only consider motion in the plane, the sum of forces in the vertical direction in Eq. (6) are assumed to be equal to zero, which defines the lift required for the UAV to maintain altitude and is given by

$$F_h = 0 \quad \Rightarrow \quad L = \frac{W}{\cos\Phi}. \tag{7}$$

2.2. Aerodynamic Model

Aerodynamic forces such as lift and drag are given by

$$L(v,\Phi) = C_L(v,\Phi)S_{ref}\frac{\rho v^2}{2}, \quad D(v,\Phi) = C_D(v,\Phi)S_{ref}\frac{\rho v^2}{2}, \tag{8}$$

where lift and drag are expressed as coefficients (as defined in the nomenclature) and depend explicitly on the values of v and Φ. Substituting Eq. (8) into Eq. (7) allows one to solve for the required lift coefficient to balance the weight of the UAV, which is given by

$$C_L(v,\Phi) = \frac{2W}{S_{ref}\rho v^2\cos\Phi}. \tag{9}$$

The drag coefficient (C_D) can be expanded into a zero lift drag component (C_{D0}) and an induced drag component as follows:

$$C_D(v,\Phi) = C_{D0} + KC_L(v,\Phi)^2. \tag{10}$$

Eq. (10) is known as a drag polar [18].

2.3. State and Control Boundaries

The minimum speed and maximum bank angle of the UAV are limited by the maximum lift coefficient $C_{L\max}$. Explicit expressions for the minimum speed and maximum bank angle of a UAV obtained from Eq. (10) are given as follows:

$$v_{\min}(\Phi) = \sqrt{\frac{2W}{S_{ref}\rho C_{L\max}\cos\Phi}} \quad \in \quad \left[\sqrt{\frac{2W}{S_{ref}\rho C_{L\max}}}, \infty\right) \tag{11}$$

$$\Phi_{\max} = \cos^{-1}\left(\frac{2W}{S_{ref}\rho v^2 C_{L\max}}\right) \tag{12}$$

The maximum speed of the UAV is defined by the speed at which drag equals the maximum thrust ($T_{\max}$) of the UAV. Starting by setting the max thrust $T_{\max}$ equal to drag and substituting in the expressions for drag given in Eq. (10) and the expression for required lift given in Eq. (9) gives an algebraic expression involving velocity. Solving for velocity gives the maximum velocity

$$v_{\max} = \sqrt{\frac{T_{\max} + \sqrt{{T_{\max}}^2 - 16C_{D0}W^2K}}{\rho C_{D0}}}, \tag{13}$$

which occurs at a bank angle of zero.

2.4. Hybrid System Model

As outlined in Section 1.2, our solution to the nonlinear control problem stated above consists of a hybrid feedback control strategy that unites two state-feedback controllers: a global controller capable of steering or transitioning the vehicle to nearby the waypoint and a local controller capable of steering the vehicle about a loitering radius. In this way, the closed-loop system resulting when applying our proposed hybrid control algorithm is a hybrid dynamical system. The state, which we denote by z, of the proposed aerial vehicle controlled by a hybrid control algorithm is given by

$$z = [x \;\; y \;\; v \;\; \Psi \;\; q]^\top \in U := \mathbb{R} \times \mathbb{R} \times [v_{\min}, v_{\max}] \times [-\pi, \pi] \times \{1, 2\} \tag{14}$$

where q is a switching variable that describes which controller is being utilized. A value $q = 2$ corresponds to the global (transit) controller and $q = 1$ corresponds to the local (loiter) controller being in the loop. The global controller will be designed to guide the vehicle at speed v_{C_2} to nearby the waypoint while the local controller will be designed to maneuver at a desired speed v_{C_1} about the loiter circle of radius R_C centered around the waypoint; see Figure 1. The parameter R_C defines the desired loiter circle radius used in the feedback law. The velocity is limited by the minimum and maximum steady level speed of the UAV ($v_{\min}$ and $v_{\max}$). For each $q \in \{1, 2\}$, the UAV's thrust (T_q) and bank angle (Φ_q) define the control inputs of the UAV and are constrained as follows:

$$(T_q, \Phi_q) \in [T_{\min}, T_{\max}] \times [-\Phi_{\max}, \Phi_{\max}]. \tag{15}$$

The switching between two controllers allows the dynamics of the UAV to be modeled as a hybrid system. The switch of controllers is a discrete event, while the motion of the UAV is a continuous flow of real time. The hybrid framework we employ in this work is presented in [6], where a generic hybrid system, $\mathcal{H}$, is given by four objects ($\mathcal{C}$,f,$\mathcal{D}$,G) defining its data:

- Flow map: a single-valued map f defining the flows (or continuous evolution) of $\mathcal{H}$;

- Flow set: a set $\mathcal{C}$ specifying the points where flows are possible;
- Jump map: a set valued map G defining the jumps (or discrete evolution) of $\mathcal{H}$;
- Jump set: a set $\mathcal{D}$ specifying the points where jumps are possible.

Then, for the control problem in this paper, a hybrid system $\mathcal{H} = (\mathcal{C}, f, \mathcal{D}, G)$ representing the closed-loop system from controlling the UAV using the transit and loiter controllers has state space U and can be written in the compact form

$$\mathcal{H}: \quad z \in U \quad \left\{ \begin{array}{lcll} \dot{z} & = & f(z, \kappa(z)) & z \in \mathcal{C} \\ z^+ & = & G(z) & z \in \mathcal{D} \end{array} \right. , \tag{16}$$

where κ is the feedback law applied to the control input of the UAV, which is given by

$$\kappa(z) = \left\{ \begin{array}{l} \kappa_1(x, y, v, \Psi) \ \text{ if } \ q = 1 \ \text{(local/loiter)} \\ \kappa_2(x, y, v, \Psi) \ \text{ if } \ q = 2 \ \text{(global/transit)}. \end{array} \right. \tag{17}$$

As it is made precise below, each feedback law has corresponding flow set ($\mathcal{C}_q$) and jump set ($\mathcal{D}_q$) that specify the domain where the control law is applied and where to switch to another control law respectively. The flow and jump map for the UAV hybrid system are given by

$$f(z, (T_q, \Phi_q)) = \begin{bmatrix} v \cos \Psi \\ v \sin \Psi \\ \frac{T_q - D(v, \Phi_q)}{m} \\ \frac{g}{v} \tan \Phi_q \\ 0 \end{bmatrix} \tag{18}$$

$$G(z) = \begin{bmatrix} x \\ y \\ v \\ \Psi \\ 3 - q \end{bmatrix} \tag{19}$$

The flow map defines a differential equation that corresponds to the equations of motion for the UAV in the plane under the effect of the feedback law, as discussed previously, and the jump map toggles which controller is commanding thrust and bank angle. The events triggering jumps are determined by the following choice of the flow and jump sets:

$$\mathcal{C} := \mathcal{C}_1 \cup \mathcal{C}_2, \qquad \mathcal{D} := \mathcal{D}_1 \cup \mathcal{D}_2$$

where

$$\mathcal{C}_1 := \{z \in U : q = 1, |R(x,y) - R_C| \leq d, R(x,y) \neq 0\}$$
$$\mathcal{C}_2 := \left\{z \in U : q = 2, \frac{1}{2}\left((R(x,y) - R_C)^2 + (v - v_{C_2})^2 + (\Psi - \Psi_{C_2}(x,y))^2\right) \geq c, R(x,y) \neq 0\right\}$$
$$\mathcal{D}_1 := \{z \in U : q = 1, |R(x,y) - R_C| \geq d, R(x,y) \neq 0\}$$
$$\mathcal{D}_2 := \left\{z \in U : q = 2, \frac{1}{2}\left((R(x,y) - R_C)^2 + (v - v_{C_2})^2 + (\Psi - \Psi_{C_2}(x,y))^2\right) \leq c, R(x,y) \neq 0\right\} \tag{20}$$

where $R(x,y) = \sqrt{x^2 + y^2}$. The flow and jump sets were selected to ensure stability of the hybrid controller. This was done by ensuring that the boundary for the global jump set ($\mathcal{D}_2$) is contained in a sub-level set of the basin of attraction induced by the local controller. The details of this selection are discussed in the uniting global and local controller section, which is Section 3.3. For the special case of $R = 0$, the hybrid system is undefined. However, solutions cannot remain at $R = 0$ because of the lower bound on velocity given in Eq. (23).

3. Design of Hybrid Controller for Transit and Loitering

The transit and loiter control laws for the UAV have different objectives. The transit control law will command a thrust to approach the loiter circle at transit velocity, while commanding a heading to point the UAV's velocity vector towards the loiter circle. In contrast, the loiter control law will command thrust (less than the maximum) to achieve the desired loiter velocity, while gradually commanding a heading to make the velocity vector of the UAV tangent to the desired loiter circle. Fig. 3 shows a block diagram of the closed-loop system where a hybrid controller performs the selection of transit and loiter mode.

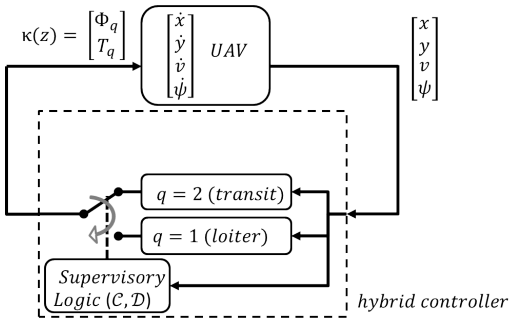

Figure 3: Control System Block Diagram.

The supervisory logic within the hybrid controller switches between the controllers to steer the UAV to the loiter circle and then loiter about it. The objective of the hybrid controller in loiter mode is to stabilize the UAV into

a loiter pattern defined by a constant radius R_C and a constant velocity v_C, which implicitly defines a desired heading Ψ_C. The target set of points for the state components of the UAV (x, y, v, Ψ) and of the controller (q) is given by

$$\mathcal{A} = \{(x, y, v, \Psi, q) \in U : R(x, y) = R_C, v = v_{C_q}, \Psi = \Psi_{C_q}(x, y), q = 1\}. \quad (21)$$

Namely, the goal is to steer R to R_C at speed v_{C_q} with $q = 1$. For both the local and global controller, an error quantity for position, velocity, and heading angle will be defined. For each $q \in \{1, 2\}$ the error is given by

$$e_q = \begin{bmatrix} e_{1,q} \\ e_{2,q} \\ e_{3,q} \end{bmatrix} := \begin{bmatrix} R(x, y) - R_C \\ v - v_{C_q} \\ \Psi - \Psi_{C_q} \end{bmatrix}. \quad (22)$$

Asymptotic stability of the set $\mathcal{A}$ will be proven using the backstepping method[17] by first showing that the system can be stabilized by controlling Ψ directly. Section 3.1 covers the proof of stability for the loiter and transit controllers individually through Ψ actuation. Section 3.2 applies the backstepping method to the results from Section 3.1 to show that both the loiter and transit controllers can be stabilized individually with actuation through Φ. Section 3.3 combines the transit and loiter controllers from Section 3.2 to create a united hybrid controller that maintains the stability properties of the individual controllers.

3.1. Control design for the case of actuation through (T, Ψ)

In this case, the state of interest becomes

$$\tilde{z} = [x \;\; y \;\; v \;\; q]^\top \in \widetilde{U} := \mathbb{R} \times \mathbb{R} \times [v_{\min}, v_{\max}] \times \{1, 2\} \quad (23)$$

and the error system is defined as

$$\tilde{e}_q = \begin{bmatrix} \tilde{e}_{1,q} \\ \tilde{e}_{2,q} \end{bmatrix} := \begin{bmatrix} R(x, y) - R_C \\ v - v_{C_q} \end{bmatrix}. \quad (24)$$

The state error equation has continuous dynamics given by

$$\dot{\tilde{e}}_q = \begin{bmatrix} \frac{x}{R(x,y)} v \cos \Psi_q + \frac{y}{R(x,y)} v \sin \Psi_q \\ \frac{T_q - D(v)}{m} \end{bmatrix} \quad (25)$$

where the control input is defined as (T_q, Ψ_q). Note that in this case, drag is only a function of velocity (*i.e.*, $D(v)$) instead of velocity and bank angle. A candidate Lyapunov function is given by[1]

$$\tilde{V}_q(\tilde{e}_q) = \frac{1}{2} \tilde{e}_q^\top \tilde{e}_q. \quad (26)$$

[1]Note that the Lyapunov function given in Eq. (26) is suitable for global asymptotic stability of the origin of the error system as it is positive definite and radially unbounded – in fact, it is lower and upper bounded by (quadratic) $\mathcal{K}_\infty$ functions.

Note that the target set of points from $\tilde{e}_q$ to stabilize is given by

$$\tilde{\mathcal{A}} = \{(x, y, v) : R(x, y) = R_C, v = v_{C_q}, q = 1\}, \tag{27}$$

and the flow and jump sets are defined as

$$\begin{aligned}
\tilde{\mathcal{C}}_1 &:= \left\{\tilde{z} \in \widetilde{U} : q = 1, |R(x, y) - R_C| \leq \tilde{d}, R \neq 0\right\} \\
\tilde{\mathcal{C}}_2 &:= \left\{\tilde{z} \in \widetilde{U} : q = 2, \frac{1}{2}\left((R(x, y) - R_C)^2 + (v - v_{C_1})^2\right) \geq \tilde{c}, R \neq 0\right\} \\
\tilde{\mathcal{D}}_1 &:= \left\{\tilde{z} \in \widetilde{U} : q = 1, |R(x, y) - R_C| \geq \tilde{d}, R \neq 0\right\} \\
\tilde{\mathcal{D}}_2 &:= \left\{\tilde{z} \in \widetilde{U} : q = 2, \frac{1}{2}\left((R(x, y) - R_C)^2 + (v - v_{C_1})^2\right) \leq \tilde{c}, R \neq 0\right\},
\end{aligned} \tag{28}$$

where

$$\tilde{c} > (v_{\max} - v_{\min})^2 \tag{29}$$

$$\tilde{d} > \sqrt{2\tilde{c}}. \tag{30}$$

Using Eq. (25), the variation of $\tilde{V}_q$ with time can be expressed as

$$\left\langle \nabla \tilde{V}_q(\tilde{e}_q), \begin{bmatrix} \frac{x}{R(x,y)} v \cos \Psi_q + \frac{y}{R(x,y)} v \sin \Psi_q \\ \frac{T_q - D(v)}{m} \end{bmatrix} \right\rangle = \dot{R}(R(x, y) - R_C) + \frac{T_q - D(v)}{m}(v - v_{C_q}). \tag{31}$$

where $\dot{R}$ is the first entry of Eq. (25). The thrust control input affects the second term in Eq. (31). To ensure that this term is negative, a simple control law is one that guarantees that the thrust is larger than the drag if the current speed is smaller than the commanded speed, that is, $v - v_{C_q} < 0$, or smaller than the drag if the current speed is larger than the current commanded speed, that is, $v - v_{C_q} > 0$. When the desired speed is achieved, that is, $v = v_{C_q}$, the thrust can be set to be equal to the drag to maintain this speed. These properties are satisfied by proportional control law, that is,

$$T_q = D(v) - k_{T_q}(v - v_{C_q}), \tag{32}$$

where $k_{T_q} > 0$. It should be noted that though Eq. (32) applies to both the global and local regions, each region may have a different target velocity (v_{Cq}), effectively creating two different controllers. Plugging the expression for the commanded thrust in Eq. (32) into Eq. (31) leads to

$$\left\langle \nabla \tilde{V}_q(\tilde{e}_q), \begin{bmatrix} \frac{x}{R(x,y)} v \cos \Psi_q + \frac{y}{R(x,y)} v \sin \Psi_q \\ \frac{T_q - D(v)}{m} \end{bmatrix} \right\rangle = \dot{R}(R(x, y) - R_C) - \frac{k_{T_q}(v - v_{C_q})^2}{m}. \tag{33}$$

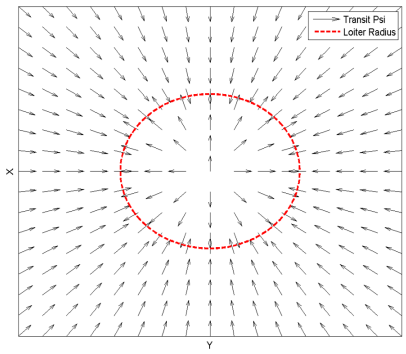

Figure 4: Quiver Plot of Global Controller Commanded Heading

3.1.1. Global/Transit Controller (q=2)

The objective of the transit (global) controller ($q = 2$) is to steer the UAV from every point in $\tilde{\mathcal{C}}_2$ to a point in ($\tilde{\mathcal{D}}_2$) in finite time, so as to switch to the loiter (local) controller. In terms of the state variables, this means pointing the velocity vector of the UAV towards the loiter radius. The value of the commanded heading in the global region ($\tilde{\mathcal{C}}_2$) is given by the control law defined as

$$\Psi_{C_2}(x,y) = \angle\left(\begin{bmatrix} \bar{x} \\ \bar{y} \end{bmatrix}\right) \qquad \forall (x,y) \in \mathbb{R}^2 \text{ such that } \tilde{z} \in \tilde{\mathcal{C}}_2 \tag{34}$$

where[2]

$$\bar{x} = \text{sign}(R_C - R(x,y))x$$
$$\bar{y} = \text{sign}(R_C - R(x,y))y$$

Note that the global heading controller is not defined on the loiter circle. This is because the local controller will be used in that region. Fig. 4 shows a quiver plot of the global controller heading with respect to a generic loiter circle. The direction of the arrows in the plot indicate the heading. The global controller commands a heading that is orthogonal and pointing towards the loiter circle.

Proposition 1. *For every function D, constant $m > 0$, velocity set-point $v_{C_2} \in [v_{\min}, v_{\max}]$, loiter radius $R_C > 0$, there exists $\gamma_2 \in \mathcal{K}_\infty$ such that the closed-loop system resulting from controlling the error system*

$$\dot{\tilde{e}}_2 = \begin{bmatrix} \frac{x}{R(x,y)} v \cos\Psi_2 + \frac{y}{R(x,y)} v \sin\Psi_2 \\ \frac{T_2 - D(v)}{m} \end{bmatrix},$$

[2]The sign function returns +1 if the input is positive, -1 if the input is negative, and 0 if the input is 0.

with the controller

$$\begin{bmatrix} T_2 \\ \Psi_2 \end{bmatrix} = \tilde{\kappa}_2(x, y, v) := \begin{bmatrix} D(v) - k_{T_2}(v - v_{C_2}) \\ \Psi_{C_2}(x, y) \end{bmatrix}, \tag{35}$$

where $k_{T_2} > 0$ *and* Ψ_{C_2} *is given in Eq. (34), is such that*

$$\left\langle \nabla \tilde{V}_2(\tilde{e}_2), \dot{\tilde{e}}_2 \right\rangle \leq -\gamma_2(|\tilde{e}_2|) \quad \textit{for all } \tilde{e}_2 \in \mathbb{R}^2 \textit{ such that } [x\ y\ v\ 2]^\top \in \tilde{\mathcal{C}}_2.$$

In particular, an appropriate choice for γ_2 *is*

$$\gamma_2(s) = \min\left\{ \frac{k_{T_2} s^2}{2m}, \frac{v_{\min} s}{\sqrt{2}} \right\} \ \ \forall s \geq 0.$$

Proof Following Eq. (33), we have that

$$\left\langle \nabla \tilde{V}_2(\tilde{e}_2), \dot{\tilde{e}}_2 \right\rangle = \dot{R}(R(x, y) - R_C) - \frac{k_{T_2}(v - v_{C_2})^2}{m},$$

where the thrust controller in Eq. (35) is already included in the second term. Substituting the expression for $\dot{R}$ given in the first entry of Eq. (25) results in

$$\left\langle \nabla \tilde{V}_2(\tilde{e}_2), \dot{\tilde{e}}_2 \right\rangle = \left(\frac{x}{R(x,y)} v \cos\Psi + \frac{y}{R(x,y)} v \sin\Psi \right) (R(x,y) - R_C) - \frac{k_{T_2}(v - v_{C_2})^2}{m}.$$

From Eq. (34) a triangle can be drawn as shown in Fig. 5 to derive

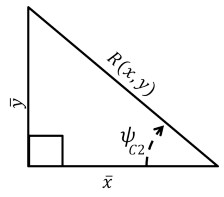

Figure 5: Global Controller Triangle

$$\cos\Psi_{C_2} = \frac{\bar{x}}{R(x,y)}, \tag{36}$$

$$\sin\Psi_{C_2} = \frac{\bar{y}}{R(x,y)}. \tag{37}$$

The substitution of Eq. (36) and Eq. (37) from the heading controller gives

$$\left\langle \nabla \tilde{V}_2(\tilde{e}_2), \dot{\tilde{e}}_2 \right\rangle = \left(\frac{x}{R(x,y)} v \frac{\bar{x}}{R(x,y)} + \frac{y}{R(x,y)} v \frac{\bar{y}}{R(x,y)} \right) (R(x,y) - R_C) - \frac{k_{T_2}(v - v_{C_2})^2}{m},$$

which can be simplified as shown below.

$$\left\langle \nabla \tilde{V}_2(\tilde{e}_2), \dot{\tilde{e}}_2 \right\rangle = v\,\text{sign}(R_C - R(x,y)) \left(\frac{x^2+y^2}{R(x,y)^2} \right) (R(x,y) - R_C) - \frac{k_{T_2}(v - v_{C_2})^2}{m}.$$
$$= v\,\text{sign}(R_C - R(x,y))(R(x,y) - R_C) - \frac{k_{T_2}(v - v_{C_2})^2}{m}.$$
$$= -v|R(x,y) - R_C| - \frac{k_{T_2}(v - v_{C_2})^2}{m}. \tag{38}$$

Substituting the error parameters from Eq. (24) into Eq. (38), namely, $\tilde{e}_2 = [\tilde{e}_{1,2}\ \tilde{e}_{2,2}]^\top$, results in

$$\left\langle \nabla \tilde{V}_2(\tilde{e}_2), \dot{\tilde{e}}_2 \right\rangle = -v|\tilde{e}_{1,2}| - \frac{k_{T_2}(\tilde{e}_{2,2})^2}{m}. \tag{39}$$

Since v is lower bounded by $v_{\min}$, γ_2 can be defined as[3]

$$\gamma_2(s) = \min \left\{ \frac{k_{T_2} s^2}{2m}, \frac{v_{\min} s}{\sqrt{2}} \right\} \quad \forall \ s \geq 0. \tag{40}$$

The first property in Proposition 1 establishes stability and uniform attractivity of the origin of the global error coordinates (e_2) for the closed-loop system using the global controller on the flow set ($\mathcal{C}_2$).

■

3.1.2. Local Controller

The objective of the local controller ($q = 1$) is to steer the state of the UAV to the desired loiter circle at the desired velocity. For the local controller, the set point velocity (v_{C_2}) used in Eq. (32) to determine the thrust input is the desired loiter speed. The expression for the local controller commanded heading shown in Eq. (42) is inspired by the control law in [1]. We incorporate a discrete dynamic parameter $p \in \{-1, 1\}$ designating the direction of rotation about the

[3] This bound follows considering the generic function $V(x) = ax_2^2 + bx_1$, where $x_1 > 0$, $a > 0$, and $b > 0$. Note if $|x_1| \geq |x_2|$ then $b|x_1| = b\max\{|x_1|, |x_2|\} = b|x|$. Since $|x| = \sqrt{x_1^2 + x_2^2} \leq \sqrt{2}|x|$, we get $b|x_1| \geq \frac{b|x|}{\sqrt{2}}$. If $|x_1| < |x_2|$ then $ax_2^2 = a|x|_\infty^2 \geq a\frac{|x|_2^2}{2} = a\frac{|x|^2}{2}$. Then we have $V(x) \geq \alpha(x) := \min\left\{a\frac{|x|^2}{2}, b\frac{|x|}{\sqrt{2}}\right\}$

loiter circle. [4] Then, the control law is defined by

$$\Psi_{C_1}(x,y) = \angle \left(\begin{bmatrix} y({R_C}^2 - R(x,y)^2) + p2xR(x,y)R_C \\ x({R_C}^2 - R(x,y)^2) - p2yR(x,y)R_C \end{bmatrix} \right) \forall (x,y) \in \mathbb{R}^2$$
$$\text{such that } \tilde{z} \in \tilde{\mathcal{C}}_1 \tag{42}$$

which is well-defined and single valued on $\tilde{\mathcal{C}}_1$. The local controller commands a

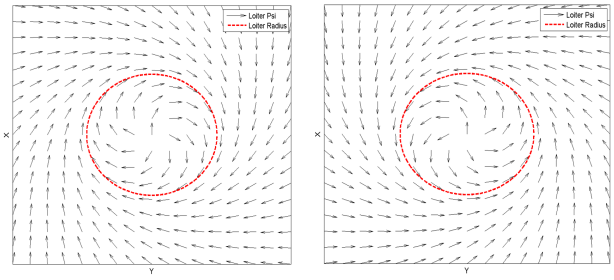

Figure 6: Quiver plot of local controller commanded heading (CW for p=1 and CCW for p=-1).

heading that gradually approaches the loiter circle tangentially and settles on an equilibrium that can rotate clockwise or counter-clockwise depending on p. Selecting $p = -1$ gives a counter-clockwise rotation, and selecting $p = 1$ gives a clockwise rotation. Fig. 6 shows a quiver plot of the local controller heading with respect to a generic loiter circle. The direction of the arrows in the plot indicate the heading.

Proposition 2. *For every constant $m > 0$, velocity set-point $v_{C_1} \in [v_{\min}, v_{\max}]$, loiter radius $R_C > 0$, and parameter $p \in \{-1, 1\}$, there exists $\gamma_1 \in \mathcal{K}_\infty$ such that the closed-loop system resulting from controlling the error system*

$$\dot{\tilde{e}}_1 = \begin{bmatrix} \frac{x}{R(x,y)} v \cos\Psi_1 + \frac{y}{R(x,y)} v \sin\Psi_1 \\ \frac{T_1 - D(v)}{m} \end{bmatrix},$$

[4] This parameter could become a state variable with discrete dynamics

$$p^+ = -p \quad \text{when} \quad \begin{cases} p = 1 \text{ and } \frac{1}{R(x,y)} \begin{bmatrix} x \\ y \end{bmatrix} \times \begin{bmatrix} \cos\Psi \\ \sin\Psi \end{bmatrix} \leq -\mu \\ p = -1 \text{ and } \frac{1}{R(x,y)} \begin{bmatrix} x \\ y \end{bmatrix} \times \begin{bmatrix} \cos\Psi \\ \sin\Psi \end{bmatrix} \geq \mu \end{cases} \tag{41}$$

and continuous dynamics $\dot{p} = 0$ where $\mu \in [0, 1]$ is a constant parameter that defines hysteresis for switching the value of p. The local controller is hybrid because of the switching of p. Switching is based on the cross product of unit position and velocity vectors as shown in Eq. (41). The selection of rotation direction in Eq. (41) utilizes the pre-existing rotation of the UAV around the loiter point based on the cross-product of the UAV's initial position and velocity vectors.

with the controller

$$\begin{bmatrix} T_1 \\ \Psi_1 \end{bmatrix} = \tilde{\kappa}_1(x, y, v) := \begin{bmatrix} D(v) - k_{T_1}(v - v_{C_1}) \\ \Psi_{C_1}(x, y) \end{bmatrix}, \tag{43}$$

where $k_{T_1} > 0$ *and* Ψ_{C_1} *is given in Eq. (42), satisfies*

$$\left\langle \nabla \tilde{V}_1(\tilde{e}_1), \dot{\tilde{e}}_1 \right\rangle \leq -\gamma_1(|\tilde{e}_1|) \quad \textit{for all } \tilde{e}_1 \in \mathbb{R}^2 \textit{ such that } [x\ y\ v\ 1]^\top \in \tilde{\mathcal{C}}_1.$$

In particular, an appropriate choice for γ_1 *is*

$$\gamma_1(s) = \min\left\{ \frac{v_{\min} R_C}{(R_C + \tilde{d})^2 + R_C^2}, \frac{k_{T_1}}{m} \right\} s^2 \qquad \forall\ s \geq 0,$$

Proof In this proof, $R(x, y)$ will be denoted as R to simplify notation. Following Eq. (33), we have that

$$\left\langle \nabla \tilde{V}_1(\tilde{e}_1), \dot{\tilde{e}}_1 \right\rangle = \dot{R}(R - R_C) - \frac{k_{T_1}(v - v_{C_1})^2}{m},$$

where the thrust controller in Eq. (43) is already included in the second term. Substituting the expression for $\dot{R}$ given in the first entry of Eq. (25) results in

$$\left\langle \nabla \tilde{V}_1(\tilde{e}_1), \dot{\tilde{e}}_1 \right\rangle = \left(\frac{x}{R} v \cos\Psi + \frac{y}{R} v \sin\Psi \right)(R - R_C) - \frac{k_{T_1}(v - v_{C_1})^2}{m}.$$

A triangle can be drawn from Eq. (42) as shown in Fig. 7 to derive expressions for the sin and cos of Ψ_{C_1}. The $\mp$ and $\pm$ have been substituted for p from Eq. (42) to account for both directions of rotation.

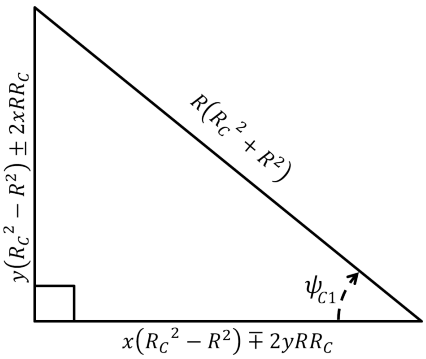

Figure 7: Local Controller Triangle

The hypotenuse of the triangle in the figure can be derived using the law of cosines starting with the expressions for the other legs of the triangle taken

from Eq. (42). The expressions in Eq. (44) and Eq. (45) follow naturally from the expression for the hypotenuse of the triangle in Fig. 7.

$$\cos\Psi_{C_1} = \frac{x(R_C^2 - R^2) \mp 2yRR_C}{R(R_C^2 + R^2)} \tag{44}$$

$$\sin\Psi_{C_1} = \frac{y(R_C^2 - R^2) \pm 2xRR_C}{R(R_C^2 + R^2)} \tag{45}$$

The further substitution of Eq. (44) and Eq. (45) from the heading controller gives

$$\left\langle \nabla\tilde{V}_1(\tilde{e}_1), \dot{\tilde{e}}_1 \right\rangle = \left(\frac{x}{R} v \left(\frac{x(R_C^2 - R^2) \mp 2yRR_C}{R(R_C^2 + R^2)} \right) + \frac{y}{R} v \left(\frac{y(R_C^2 - R^2) \pm 2xRR_C}{R(R_C^2 + R^2)} \right) \right) \times (R - R_C) - \frac{k(v - v_{C_1})^2}{m}.$$

This expression can be simplified as shown below

$$\begin{aligned}
\left\langle \nabla\tilde{V}_1(\tilde{e}_1), \dot{\tilde{e}}_1 \right\rangle &= \frac{v(R_C^2 - R^2)}{(R^2 + R_C^2)}(R - R_C) - \frac{k_{T_1}(v - v_{C_1})^2}{m}. \\
\left\langle \nabla\tilde{V}_1(\tilde{e}_1), \dot{\tilde{e}}_1 \right\rangle &= \frac{v(R_C + R)(R_C - R)}{(R^2 + R_C^2)}(R - R_C) - \frac{k_{T_1}(v - v_{C_1})^2}{m}. \\
\left\langle \nabla\tilde{V}_1(\tilde{e}_1), \dot{\tilde{e}}_1 \right\rangle &= -\frac{v(R + R_C)(R - R_C)^2}{(R^2 + R_C^2)} - \frac{k_{T_1}(v - v_{C_1})^2}{m}.
\end{aligned} \tag{46}$$

Substituting the error parameters from Eq. (24) into Eq. (46) namely, $\tilde{e}_1 = [\tilde{e}_{1,1}\ \tilde{e}_{2,1}]^\top$ results in

$$\left\langle \nabla\tilde{V}_1(\tilde{e}_1), \dot{\tilde{e}}_1 \right\rangle = -\frac{v(R + R_C)(\tilde{e}_{1,1})^2}{(R^2 + R_C^2)} - \frac{k_{T_1}(\tilde{e}_{2,1})^2}{m}, \tag{47}$$

which allows the definition of γ_1 as

$$\gamma_1(s) = \min\left\{ \frac{v_{\min} R_C}{(R_C + \tilde{d})^2 + R_C^2}, \frac{k_{T_1}}{m} \right\} s^2 \qquad \forall\ s \geq 0, \tag{48}$$

■

Then, the origin of the local error coordinates $(\tilde{e}_1)$ for the closed-loop system implementing the local controller on the flow set $(\tilde{\mathcal{C}}_1)$ is asymptotically stable. Since the origin of $\tilde{e}_1$ corresponds to the points (x, y) in the loiter circle and loiter velocity equal to v_{C_q}, this also implies that the heading of the UAV on the loiter circle is tangent to the loiter circle as illustrated in Fig. 6.

The following result establishes that, for each $q \in \{1, 2\}$, the constraint $[T_{\min}, T_{\max}]$ is forward invariant under the feedback laws in (35) and (43) assigning T .

Lemma 1. *Under the effect of (32), $\tilde{e}_{2,q}$ evolves according to*

$$\dot{\tilde{e}}_{2,q} = -\frac{k_{T_q}}{m}\tilde{e}_{2,q}$$

and, since $\frac{k_{T_q}}{m} > 0$, we have that $\tilde{e}_{2,q} = 0$ is globally asymptotically stable. Furthermore, every solution to this subsystem with $T_q(0) \in [T_{\min}, T_{\max}]$ is such that

$$T_q(t) \in [T_{\min}, T_{\max}] \qquad \forall t \geq 0. \tag{49}$$

Remark The stability property of the origin (for $\tilde{e}_{2,q}$) follows directly from the resulting dynamics of $\tilde{e}_{2,q}$, which are obtained by plugging (32) into $\dot{\tilde{e}}_{2,q}$. In fact, under such feedback,

$$\tilde{e}_{2,q}(t) = \tilde{e}_{2,q}(0)e^{-\frac{k_{T_q}}{m}t} \qquad \forall t \geq 0 \tag{50}$$

for any initial condition $\tilde{e}_{2,q}(0)$. The property in (49) is a consequence of the resulting form of T in (32), since the substitution of (50) into (32) gives

$$T = D(v) - \tilde{e}_{2,q}(0)e^{-\frac{k_{T_q}}{m}t} \tag{51}$$

3.2. Control design for the case of actuation through (T, Φ) via backstepping

The results in the previous section establish properties of the UAV when Ψ is a control input. However, for the hybrid system with flow map given in Eq. (18), Ψ is a function of the control input Φ. Using the method of backstepping, asymptotic stability will be proved for the hybrid system with Φ as a control input. Recalling the error system given in Eq. (25), and adding and subtracting the desired heading Ψ_{Cq} from the heading state Ψ, we obtain

$$\dot{e}_q = \begin{bmatrix} \frac{x}{R(x,y)}v\cos\left(\Psi - \Psi_{C_q} + \Psi_{C_q}\right) + \frac{y}{R(x,y)}v\sin\left(\Psi - \Psi_{C_q} + \Psi_{C_q}\right) \\ \frac{T_q - D(v,\Phi)}{m} \end{bmatrix}.$$

Now recall $e_{3,q}$ from Eq. (22) as the difference between the current heading Ψ and the commanded heading Ψ_{C_q} and evaluate its derivative, that is,

$$\begin{aligned} e_{3,q} &= \Psi - \Psi_{C_q} \\ \dot{e}_{3,q} &= \dot{\Psi} - \left\langle \nabla_z \Psi_{C_q}(z), f(z, \kappa(z)) \right\rangle, \end{aligned}$$

where, according to Eq. (18),

$$\dot{\Psi} = \frac{g}{v}\tan\Phi_q.$$

The dynamics of e_q are then

$$\dot{e}_q = \begin{bmatrix} \frac{x}{R(x,y)}v\cos\left(e_{3,q} + \Psi_{C_q}\right) + \frac{y}{R(x,y)}v\sin\left(e_{3,q} + \Psi_{C_q}\right) \\ \frac{T_q - D(v,\Phi)}{m} \\ \frac{g}{v}\tan\Phi_q - \left\langle \nabla_z \Psi_{C_q}(z), f(z, \kappa(z)) \right\rangle \end{bmatrix}. \tag{52}$$

Using

$$V_q(e_q) = \tilde{V}_q(\tilde{e}_q) + \frac{1}{2}{e_{3,q}}^2 \tag{53}$$

for a Lyapunov function candidate, the derivative can be expressed as

$$\begin{aligned}
\langle \nabla V_q(e_q), \dot{e}_q \rangle &= \left(\frac{x}{R} v \cos\left(e_{3,q} + \Psi_{C_q}\right) + \frac{y}{R} v \sin\left(e_{3,q} + \Psi_{C_q}\right) \right) (R - R_C) \\
&\quad - \frac{k_{T_q}(v - v_{C_q})^2}{m} + e_{3,q} \left(\frac{g}{v} \tan \Phi_q - \left\langle \nabla_z \Psi_{C_q}(z), f(z, \kappa(z)) \right\rangle \right) \\
\langle \nabla V_q(e_q), \dot{e}_q \rangle &= \left(\frac{x}{R(x,y)} v \left(\cos e_{3,q} \cos \Psi_{C_q} - \sin e_{3,q} \sin \Psi_{C_q} \right) \right. \\
&\quad \left. + \frac{y}{R(x,y)} v \left(\sin e_{3,q} \cos \Psi_{C_q} + \cos e_{3,q} \sin \Psi_{C_q} \right) \right) \\
&\quad \times (R(x,y) - R_C) - \frac{k_{T_q}(v - v_{C_q})^2}{m} \\
&\quad + e_{3,q} \left(\frac{g}{v} \tan \Phi_q - \left\langle \nabla_z \Psi_{C_q}(z), f(z, \kappa(z)) \right\rangle \right)
\end{aligned} \tag{54}$$

From here, the control input Φ_q can be formulated for the specific global and local controllers to make the origin asymptotically stable for the system in Eq. (52) on the set $U \setminus \{z : R(x,y) = 0\}$.

3.2.1. Global Controller Backstepping

The global controller is designed to make the origin of the error system e_q asymptotically stable. This is achieved by inverting the tangent function containing Φ_2, the control input, and compensating for positive terms that come when differentiating the Lyapunov function. This results in the controller

$$\begin{aligned}
&\Phi_{C_2}(x, y, v, \Psi, e_{3,2}) \\
&\quad = \tan^{-1}\left(-\frac{k_{\Phi_2}(x, y, v, e_{3,2}) v e_{3,2}}{g} + \frac{v}{g} \left\langle \nabla_z \Psi_{C_2}(z), f(z, \kappa_2(x, y, v, \Psi)) \right\rangle \right) \\
&\quad = \tan^{-1}\left(-\frac{k_{\Phi_2}(x, y, v, e_{3,2}) v e_{3,2}}{g} - \frac{y v^2}{g R(x,y)^2} \cos \Psi + \frac{x v^2}{g R(x,y)^2} \sin \Psi \right),
\end{aligned} \tag{55}$$

where the function k_{Φ_2} is of the form

$$k_{\Phi_2}(x, y, v, e_{3,2}) = \nu + \xi(e_{3,2}) v |R(x,y) - R_C|, \tag{56}$$

$\nu > 0$, and $s \mapsto \xi(s)$ such that for each $s \in \mathbb{R}$

$$\xi(s) > \frac{1}{2} \text{ if } |s| \geq \frac{\pi}{2} \text{ and } \xi(s) \geq 0 \text{ if } |s| < \frac{\pi}{2}. \tag{57}$$

With the proposed definition of the function ξ we have that there exists $\beta \in (0,1)$ *s.t.* $\cos s + \xi s^2 \geq \beta$.[5] Making the gain k_{Φ_2} a function of the system state

[5] The definition of $\zeta \geq 0$ for $s \in (\frac{-\pi}{2} \frac{\pi}{2})$ implies that $\zeta s^2 \geq 0$ and, since $\cos s > 0$, on this region we have the existence of such $\beta > 0$. For the case when $|s| \geq \frac{\pi}{2}$, we can solve

allows for additional compensation for terms that arise when differentiating the Lyapunov function. Different values of ν and ξ can be selected, still satisfying the constraints in Eq. (57), as $e_{3,2}$ approaches zero, to prevent chattering of the controller commands.

Proposition 3. *For every constant $m > 0$, velocity set-point $v_{C_2} \in [v_{\min}, v_{\max}]$, and loiter radius $R_C > 0$, there exists $\gamma_2 \in \mathcal{K}_\infty$ such that the closed-loop system resulting from controlling the error system*

$$\dot{e}_2 = \begin{bmatrix} \frac{x}{R(x,y)} v \cos\left(e_{3,2} + \Psi_{C_2}\right) + \frac{y}{R(x,y)} v \sin\left(e_{3,2} + \Psi_{C_2}\right) \\ \frac{T_2 - D(v,\Phi)}{m} \\ \frac{g}{v} \tan \Phi_2 - \langle \nabla_z \Psi_{C_2}(z), f(z, \kappa_2(z)) \rangle \end{bmatrix}, \tag{58}$$

with the controller

$$\begin{bmatrix} T_2 \\ \Phi_2 \end{bmatrix} = \kappa_2(x, y, v, \Psi, \Psi_{C_2}) := \begin{bmatrix} D(v,\Phi) - k_{T_2}(v - v_{C_2}) \\ \Phi_{C_2}(x, y, v, \Psi, e_{3,2}) \end{bmatrix}, \tag{59}$$

where $k_{T_2} > 0$, Ψ_{C_2} is given in Eq. (34), and Φ_{C_2} is given in Eq. (55), satisfies

1. $\langle \nabla V_2(e_2), \dot{e}_2 \rangle \leq -\gamma_2(|e_2|)$ *for all* $e_2 \in \mathbb{R}^3$ *such that* $[x\ y\ v\ \Psi]^\top \in \mathcal{C}_2$

In particular, an appropriate choice of γ_2 is

$$\gamma_2(s) = \min\left\{ \frac{v_{\min}\beta s}{\sqrt{3}}, \frac{k_{T_2} s^2}{3m}, \frac{\nu s^2}{3} \right\} \ \forall s \geq 0.$$

Proof In this proof, $R(x, y)$ will be denoted as R to simplify notation. Substituting in Eq. (54) the expressions for $\cos \Psi_{C_2}$ and $\sin \Psi_{C_2}$ given in Eq. (36) and Eq. (37) gives

$$\begin{aligned} \langle \nabla V_2(e_2), \dot{e}_2 \rangle = &\left(\frac{x}{R} v \left(\cos e_{3,2} \frac{x}{R} - \sin e_{3,2} \frac{y}{R} \right) + \frac{y}{R} v \left(\sin e_{3,2} \frac{x}{R} + \cos e_{3,2} \frac{y}{R} \right) \right) (R - R_C) \\ &- \frac{k_{T_2}(v - v_{C_2})^2}{m} + e_{3,2} \left(\frac{g}{v} \tan \Phi_2 - \langle \nabla_z \Psi_{C_2}(z), f(z, \kappa_2(z)) \rangle \right) \\ = &- \left(v \left(\cos e_{3,2} \frac{x^2}{R^2} \right) + v \left(\cos e_{3,2} \frac{y^2}{R^2} \right) \right) \operatorname{sign}(R - R_C)(R - R_C) \\ &- \frac{k_{T_2}(v - v_{C_2})^2}{m} + e_{3,2} \left(\frac{g}{v} \tan \Phi_2 - \langle \nabla_z \Psi_{C_2}(z), f(z, \kappa_2(z)) \rangle \right) \\ = &- v|R - R_C| \cos e_{3,2} - \frac{k_{T_2}(v - v_{C_2})^2}{m} \\ &+ e_{3,2} \left(\frac{g}{v} \tan \Phi_2 - \langle \nabla_z \Psi_{C_2}(z), f(z, \kappa_2(z)) \rangle \right). \end{aligned} \tag{60}$$

for the inflection point by taking derivatives, which gives $\sin s + 2\zeta s = 0$, or equivalently, $\frac{\sin s}{s} = -2\zeta$. Selecting $\zeta > 1/2$ moves the inflection point to $s \in (\frac{-\pi}{2}\ \frac{\pi}{2})$ due to the fact that $\frac{\sin s}{s} \leq 1\ \forall\ |s| \geq \frac{\pi}{2}$. As a consequence, there exists a lower bound $\beta \in (0, 1)$ as required..

Taking the partial derivative of Ψ_{C_2} with respect to the hybrid system state and computing the dot product with the global flow map gives

$$\begin{aligned}\langle \nabla_z \Psi_{C_2}(z), f(z, \kappa_2(z)) \rangle &= \begin{bmatrix} \frac{-y}{R^2} & \frac{x}{R^2} & 0 & 0 & 0 \end{bmatrix}^\top \begin{bmatrix} v\cos\Psi & v\sin\Psi & \frac{T_2 - D}{m} & \frac{g}{v}\tan\Phi_2 & 0 \end{bmatrix} \\ &= -\frac{yv}{R^2}\cos\Psi + \frac{xv}{R^2}\sin\Psi, \end{aligned} \tag{61}$$

which can be substituted into Eq. (60) resulting in

$$\begin{aligned}\langle \nabla V_2(e_2), \dot{e}_2 \rangle = &- v|R - R_C|\cos e_{3,2} - \frac{k_{T_2}(v - v_{C_2})^2}{m} \\ &+ e_{3,2}\left(\frac{g}{v}\tan\Phi_2 + \frac{yv}{R^2}\cos\Psi - \frac{xv}{R^2}\sin\Psi\right).\end{aligned}$$

Since $R \neq 0$, the further substitution of the Φ_{C_2} controller defined in Eq. (55) simplifies the expression further to

$$\langle \nabla V_2(e_2), \dot{e}_2 \rangle = - v|R - R_C|\cos e_{3,2} - \frac{k_{T_2}(v - v_{C_2})^2}{m} - k_{\Phi_2}(x, y, v, e_{3,2})e_{3,2}^2. \tag{62}$$

The expression in Eq. (56) for $k_{\Phi 2}$ and the error terms from Eq. (22) can be substituted to give

$$\begin{aligned}\langle \nabla V_2(e_2), \dot{e}_2 \rangle &= - v|R - R_C|\cos e_{3,2} - \frac{k_{T_2}(v - v_{C_2})^2}{m} - (\nu + \xi v|R - R_C|)e_{3,2}^2 \\ &= - v|e_{1,2}|\left(\cos(e_{3,2}) + \xi e_{3,2}^2\right) - \frac{k_{T_2}e_{2,2}^2}{m} - \nu e_{3,2}^2\end{aligned}$$

Since $\cos(e_{3,2}) + \xi e_{3,2}^2 \geq \beta$ as defined by Eq. (57), we have, for each e_2

$$\langle \nabla V_2(e_2), \dot{e}_2 \rangle \leq -v|e_{1,2}|\beta - \frac{k_{T_2}e_{2,2}^2}{m} - \nu(e_{3,2})^2 \leq -\gamma_2(|e_2|). \tag{63}$$

where γ_2 is

$$\gamma_2(s) = \min\left\{\frac{v_{\min}\beta s}{\sqrt{3}}, \frac{k_{T_2}s^2}{3m}, \frac{\nu s^2}{3}\right\} \ \forall s \geq 0.^6 \tag{64}$$

■

[6] This bound follows considering the generic function $V(x) = \nu x_3^2 + \beta x_2^2 + \gamma x_1$, where $x_1 > 0$, $\beta > 0$ and $\nu > 0$. If $|x_1| \geq |x_2|$ and $|x_1| \geq |x_3|$ then $\gamma|x_1| = \gamma\max\{|x_1|, |x_2|, |x_3|\} = \gamma|x|_\infty$. Since $|x| = \sqrt{x_1^2 + x_2^2 + x_3^2} \leq \sqrt{3}|x|_\infty$, we get $\gamma|x_1| \geq \frac{\gamma|x|}{\sqrt{3}}$. Also, if $|x_2| > |x_1|$ and $|x_2| > |x_3|$ then $\beta x_2^2 = \beta|x|_\infty^2 \geq \beta\frac{|x|^2}{3} = \beta\frac{|x|^2}{3}$. Similarly, if $|x_3| > |x_1|$ and $|x_3| > |x_2|$ then $\nu x_3^2 = \nu|x|_\infty^2 \geq \nu\frac{|x|^2}{\sqrt{3}^2} = \nu\frac{|x|^2}{\sqrt{3}^2}$. Then we have $V(x) \geq \alpha(|x|) := \min\left\{\nu\frac{|x|^2}{3}, \beta\frac{|x|^2}{3}, \frac{\gamma|x|}{\sqrt{3}}\right\}$

3.2.2. Local Controller Backstepping

Similar to the global controller, the local controller is designed to make the origin of the error system asymptotically stable. This is achieved by inverting the tangent function containing Φ_1, the control input, and compensating for positive terms that come when differentiating the Lyapunov function. In this way the proposed controller is given by

$$\begin{aligned}
&\Phi_{C_1}(x, y, \Psi, \Psi_{C_1}) \\
&\quad = \tan^{-1}\left[-\frac{k_{\Phi_1}(x, y, v, \Psi, \Psi_{C_1})ve_{3,1}}{g} + \frac{v}{g}\left\langle \nabla_z \Psi_{C_1}(z), f(z, \kappa_1(z))\right\rangle\right] \\
&\quad = \tan^{-1}\left[-\frac{k_{\Phi_1}(x, y, v, \Psi, \Psi_{C_1})ve_{3,1}}{g} - \frac{yv^2}{gR(x,y)^2}\cos\Psi + \frac{xv^2}{gR(x,y)^2}\sin\Psi\right]
\end{aligned} \tag{65}$$

where k_{Φ_1} is given by

$$\begin{aligned}
k_{\Phi_1}(x, y, v, \Psi, \Psi_{C_1}) =& \chi + \gamma(e_{3,1})v\frac{(R_C + R(x,y))(R(x,y) - R_C)^2}{R_C^2 + R(x,y)^2} \\
&+ \frac{|\sin e_{3,1}|}{\zeta^2} v 2R(x,y)R_C|p|\frac{|R(x,y) - R_C|}{R_C^2 + R(x,y)^2}
\end{aligned} \tag{66}$$

where $\chi > 0$, $\zeta \in (0, \frac{\pi}{2})$ and $s \mapsto \gamma(s)$ is a smooth function such that

$$\gamma(s) > \frac{1}{2} \text{ if } |s| \geq \frac{\pi}{2}, \text{ and } \gamma(s) \geq 0 \text{ if } |s| < \frac{\pi}{2}. \tag{67}$$

With the proposed definition of the function γ we have that there exists $\beta \in (0, 1)$ *s.t.* $\cos s + \gamma(s)s^2 \geq \beta \ \forall s \geq 0$. Note that making the "gain" k_{Φ_1} a function of the system's state allows for additional compensation of terms that arise when differentiating the Lyapunov function V_1.

Proposition 4. *For every constant $m > 0$, velocity set-point $v_{C_1} \in [v_{\min}, v_{\max}]$, loiter radius $R_C > 0$, there exists $\gamma_1 \in \mathcal{K}_\infty$ such that the closed-loop system resulting from controlling the error system*

$$\dot{e}_1 = \begin{bmatrix} \frac{x}{R(x,y)} v\cos(e_{3,1} + \Psi_{C_1}) + \frac{y}{R(x,y)} v\sin(e_{3,1} + \Psi_{C_1}) \\ \frac{T_1 - D(v,\Phi_1)}{m} \\ \frac{g}{v}\tan\Phi_1 - \left\langle \nabla_z \Psi_{C_1}(z), f(z, \kappa_1(z))\right\rangle \end{bmatrix},$$

with the controller

$$\begin{bmatrix} T_1 \\ \Phi_1 \end{bmatrix} = \kappa_1(x, y, v, \Psi, \Psi_{C_1}) := \begin{bmatrix} D(v, \Phi_1) - k_{T_1}(v - v_{C_1}) \\ \Phi_{C_1}(x, y, \Psi, \Psi_{C_1}) \end{bmatrix}, \tag{68}$$

where $k_{T_1} > 0$ and Ψ_{C_1} is given in Eq. (42) and Φ_{C_1} is given in Eq. (65), satisfies, for each $\epsilon > 0$,

1. $\langle \nabla V_1(e_1), \dot{e}_1\rangle \leq -\gamma_1(|e_1|) + \epsilon$ *for all* $e_1 \in \mathbb{R}^3$ *such that* $[x\ y\ v\ \Psi]^\top \in \mathcal{C}_1$

where ζ is chosen such that

$$\frac{v_{\max} d}{R_C} 2(R_C + d)|\sin\zeta| < \epsilon \tag{69}$$

In particular, an appropriate choice of γ_1 is

$$\gamma_1(s) = \min\left\{ \frac{v_{\min}\beta R_C}{(R_C^2 + (R_C + d)^2)}, \frac{k_{T_1}}{m}, \chi \right\} s^2 \qquad \forall s \geq 0$$

Proof In this proof, $R(x, y)$ will be denoted as R to simplify notation. Substituting in Eq. (54) the expressions for $\cos\Psi_{C_2}$ and $\sin\Psi_{C_2}$ given in Eq. (44) and Eq. (45) gives

$$\begin{aligned}
\langle \nabla V_1(e_1), \dot{e}_1 \rangle = & \left(\frac{x}{R} v \left(\cos e_{3,1} \frac{x(R_C^2 - R^2) - p2yRR_C}{R(R_C^2 + R^2)} - \sin e_{3,1} \frac{y(R_C^2 - R^2) + p2xRR_C}{R(R_C^2 + R^2)} \right) \right. \\
& \left. + \frac{y}{R} v \left(\sin e_{3,1} \frac{x(R_C^2 - R^2) - p2yRR_C}{R(R_C^2 + R^2)} + \cos e_{3,1} \frac{y(R_C^2 - R^2) + p2xRR_C}{R(R_C^2 + R^2)} \right) \right) \\
& \times (R - R_C) \\
& - \frac{k_{T_1}(v - v_{C_1})^2}{m} + e_{3,1} \left(\frac{g}{v} \tan\Phi_1 - \langle \nabla_z \Psi_{C_1}(z), f(z, \kappa_1(z)) \rangle \right)
\end{aligned} \tag{70}$$

which can be simplified to

$$\begin{aligned}
\langle \nabla V_1(e_1), \dot{e}_1 \rangle = & \left(v \cos e_{3,1} \frac{R_C^2 - R^2}{R_C^2 + R^2} - vp \sin e_{3,1} \frac{2RR_C}{R_C^2 + R^2} \right) (R - R_C) - \frac{k_{T_1}(v - v_{C_1})^2}{m} \\
& + e_{3,1} \left(\frac{g}{v} \tan\Phi_1 - \langle \nabla_z \Psi_{C_1}(z), f(z, \kappa_1(z)) \rangle \right) \\
= & \frac{v(R - R_C)}{R_C^2 + R^2} \left(\cos e_{3,1}(R_C^2 - R^2) - p2RR_C \sin e_{3,1} \right) - \frac{k_{T_1}(v - v_{C_1})^2}{m} \\
& + e_{3,1} \left(\frac{g}{v} \tan\Phi_1 - \langle \nabla_z \Psi_{C_1}(z), f(z, \kappa_1(z)) \rangle \right).
\end{aligned} \tag{71}$$

Taking the partial derivative of Ψ_{C_1} with respect to the hybrid system state

gives

$$\begin{aligned}
\frac{\partial \Psi_{C_1}}{\partial x} &= \frac{\partial \tan^{-1} \frac{y({R_C}^2-R^2)+p2xRR_C}{x({R_C}^2-R^2)-p2yRR_C}}{\partial x} \\
&= \frac{1}{1+(\frac{y({R_C}^2-R^2)+p2xRR_C}{x({R_C}^2-R^2)-p2yRR_C})^2} \\
&\quad \times \left(\frac{p2RR_C(x({R_C}^2-R^2)-p2yRR_C)-({R_C}^2-R^2)(y({R_C}^2-R^2)+p2xRR_C)}{(x({R_C}^2-R^2)-p2yRR_C)^2} \right) \\
&= \frac{-4yR^2R_C^2-y({R_C}^2-R^2)^2}{R^2({R_C}^2-R^2)^2+4R^4R_C^2} = \frac{-y}{R^2} \\
\frac{\partial \Psi_{C_1}}{\partial y} &= \frac{\partial \tan^{-1} \frac{y({R_C}^2-R^2)+p2xRR_C}{x({R_C}^2-R^2)-p2yRR_C}}{\partial y} \\
&= \frac{1}{1+(\frac{y({R_C}^2-R^2)+p2xRR_C}{x({R_C}^2-R^2)-p2yRR_C})^2} \\
&\quad \times \left(\frac{(x({R_C}^2-R^2)-p2yRR_C)+p2RR_C({R_C}^2-R^2)(y({R_C}^2-R^2)+p2xRR_C)}{(x({R_C}^2-R^2)-p2yRR_C)^2} \right) \\
&= \frac{4xR^2R_C^2+x({R_C}^2-R^2)^2}{R^2({R_C}^2-R^2)^2+4R^4R_C^2} = \frac{x}{R^2}.
\end{aligned}$$

Then, computing the dot product with the local flow map gives

$$\begin{aligned}
\langle \nabla_z \Psi_{C_1}(z), f(z,\kappa_1(z)) \rangle &= \begin{bmatrix} \frac{-y}{R^2} & \frac{x}{R^2} & 0 & 0 & 0 \end{bmatrix}^\top \begin{bmatrix} v\cos\Psi & v\sin\Psi & \frac{T_1 - D(v,\Phi)}{m} & \frac{g}{v}\tan\Phi_1 & 0 \end{bmatrix} \\
&= \frac{-yv}{R^2}\cos\Psi + \frac{xv}{R^2}\sin\Psi, \qquad (72)
\end{aligned}$$

which can be substituted into Eq. (71) resulting in

$$\begin{aligned}
\langle \nabla V_1(e_1), \dot{e}_1 \rangle = \frac{v(R-R_C)}{R_C^2+R^2}\left(\cos e_{3,1}(R_C^2-R^2) - p2RR_C\sin e_{3,1}\right) - \frac{k_{T_1}(v-v_{C_1})^2}{m} \\
+ e_{3,1}\left(\frac{g}{v}\tan\Phi_1 + \frac{yv}{R^2}\cos\Psi - \frac{xv}{R^2}\sin\Psi\right)
\end{aligned}$$

Since $R \neq 0$, further substituting the local controller given in Eq. (65) and grouping terms results in

$$\begin{aligned}
\langle \nabla V_1(e_1), \dot{e}_1 \rangle &= \frac{v(R-R_C)}{R_C^2+R^2}\left(\cos e_{3,1}(R_C^2-R^2) - p2RR_C\sin e_{3,1}\right) \\
&\quad - \frac{k_{T_1}(v-v_{C_1})^2}{m} - k_{\Phi 1}e_{3,1}^2 \\
&= -\frac{v(R-R_C)^2}{R_C^2+R^2}\cos e_{3,1}(R_C+R) - \frac{v(R-R_C)}{R_C^2+R^2}p2RR_C\sin e_{3,1} \\
&\quad - \frac{k_{T_1}(v-v_{C_1})^2}{m} - k_{\Phi 1}e_{3,1}^2
\end{aligned}$$

Substituting the definition of the gain function in (66) results in

$$\begin{aligned}\langle \nabla V_1(e_1), \dot{e}_1 \rangle = &- \frac{v(R-R_C)^2}{R_C^2+R^2}(\cos e_{3,1} + \gamma(e_{3,1})e_{3,1}^2)(R_C+R) \\ &- \frac{v(R-R_C)}{R_C^2+R^2} p 2RR_C \sin e_{3,1} \left(1 + sign\,(R-R_C)\, sign\,(\sin e_{3,1})\, p \frac{{e_{3,1}}^2}{\zeta^2}\right) \\ &- \frac{k_{T_1}(v-v_{C_1})^2}{m} - \chi e_{3,1}^2. \end{aligned} \tag{73}$$

For the case of $\text{sign}\,(R-R_C)\,\text{sign}\,(\sin e_{3,1})\,p \geq 0$ we have

$$\begin{aligned}\langle \nabla V_1(e_1), \dot{e}_1 \rangle = &- \frac{v(R-R_C)^2}{R_C^2+R^2}(\cos e_{3,1} + \gamma(e_{3,1})e_{3,1}^2)(R_C+R) \\ &- \frac{v|R-R_C|}{R_C^2+R^2} 2RR_C |\sin e_{3,1}| \left(1 + \frac{{e_{3,1}}^2}{\zeta^2}\right) \\ &- \frac{k_{T_1}(v-v_{C_1})^2}{m} - \chi e_{3,1}^2. \end{aligned}$$

Substituting the error terms from Eq. (22) and the bound from Eq. (67) means that the expression can be bounded by

$$\langle \nabla V_1(e_1), \dot{e}_1 \rangle \leq -\frac{v(e_{1,1})^2}{R_C^2+R^2}\beta(R_C+R) - \frac{k_{T_1}(e_{2,1})^2}{m} - \chi(e_{3,1})^2 \leq -\gamma_1(|e_1|)$$

where γ_1 is defined as

$$\gamma_1(s) = \min\left\{\frac{v_{\min}\beta R_C}{(R_C^2+(R_C+d)^2)}, \frac{k_{T_1}}{m}, \chi\right\} s^2 \qquad \forall s \geq 0 \tag{74}$$

For the case of $sign\,(R-R_C)\,sign\,(\sin e_{3,1})\,p < 0$ Eq. (73) can be bounded by

$$\begin{aligned}\langle \nabla V_1(e_1), \dot{e}_1 \rangle \leq &- \frac{v(R-R_C)^2}{R_C^2+R^2}\beta(R_C+R) - \frac{v|R-R_C|}{R_C^2+R^2} 2RR_C |\sin e_{3,1}| \left(\frac{{|e_{3,1}|}^2}{\zeta^2} - 1\right) \\ &- \frac{k_{T_1}(v-v_{C_1})^2}{m} - \chi e_{3,1}^2 \end{aligned} \tag{75}$$

where we have used Eq. (67). For Eq. (75), when $|e_{3,1}| \geq \zeta$, the bound given in Eq. (74) holds. The case of $|e_{3,1}| < \zeta$ defines the value of ϵ given in Proposition 4. For this case we have

$$\begin{aligned}\langle \nabla V_1(e_1), \dot{e}_1 \rangle = &- \frac{v(R-R_C)^2}{R_C^2+R^2}(\cos e_{3,1} + \gamma(e_{3,1})e_{3,1}^2)(R_C+R) \\ &+ \frac{v|R-R_C|}{R_C^2+R^2} 2RR_C |\sin e_{3,1}| \left(1 - \frac{{e_{3,1}}^2}{\zeta^2}\right) \\ &- \frac{k_{T_1}(v-v_{C_1})^2}{m} - \chi e_{3,1}^2. \end{aligned}$$

Where the second term from the right hand side can upper bounded as

$$\frac{v|R-R_C|}{R_C^2+R^2}2RR_C|\sin e_{3,1}|\left(1-\frac{{e_{3,1}}^2}{\zeta^2}\right) < \frac{v_{\max}d}{R_C}2(R_C+d)|\sin\zeta| \qquad \forall|e_{3,1}|<\zeta. \tag{76}$$

Given $\epsilon > 0$ and the bound in Eq. (76) pick $\zeta \in (0, \frac{\pi}{2})$ such that Eq. (69) holds. Then

$$\langle \nabla V_1(e_1), \dot{e}_1\rangle \leq -\gamma_1(|e_1|)+\epsilon \text{ for all } e_1 \in \mathbb{R}^3 \text{ such that } [x\ y\ v\ \Psi]^\top \in \mathcal{C}_1$$

where γ_1 is

$$\gamma_1(s) = \min\left\{\frac{v_{\min}\beta R_C}{(R_C^2+(R_C+d)^2)}, \frac{k_{T_1}}{m}, \chi\right\}s^2 \qquad \forall s \geq 0$$

■

3.3. Uniting Global and Local Controller

The global and local controllers proposed in Section 3.1 are united using a hybrid controller with a logic variable $q \in \{1, 2\}$ leading to the closed-loop system in Eq. (16); see [6, Example 3.23] for a similar formulation. The construction in Eqs. (17)-(20) of the closed loop in Eq. (16) is such that the sets $\mathcal{C}_1, \mathcal{C}_2, \mathcal{D}_1$, and $\mathcal{D}_2$ determine when switches between the local and global controllers should occur. The definitions of these sets depend on the positive parameters c and d. The flow and jump sets can either have a disk shape ($c \geq R_C$) or an elliptical shape ($c < R_C$) depending on the values selected for c and d. Next, we provide a design methodology for these parameters.

For starters, the parameter c is chosen so that jumps from using the global controller ($q = 2$) to using the local controller ($q = 1$) occur at points in $\mathcal{D}_2$ that are also in the c-sublevel set of V_1, where V_1 is defined in (53). More precisely, we design c such that

$$\mathcal{D}_2 \subset \mathcal{L}_{V_1}(c) \tag{77}$$

where

$$\mathcal{L}_{V_1}(c) := \{(x, y, v, \Psi) \in \mathbb{R}\times\mathbb{R}\times[v_{\min}, v_{\max}]\times[-\pi,\pi] \ :\ V_1(e_1) \leq c\}$$

The set $\mathcal{D}_2$ is defined in (20) as the c-sublevel of $e_2 \mapsto V_2(e_2)$, and, as established by Proposition 3, is globally attractive. In this way, since $\mathcal{C}_2$ is the closed complement of $\mathcal{D}_2$ for $q = 2$ and $c > 0$, we have that solutions from $\mathcal{C}_2$ reach $\mathcal{D}_2$ in finite time. Then, from points z in $\mathcal{D}_2$, which due to our construction in Eq. (77) are points that are also in $\mathcal{L}_{V_1}(c)$, we have that $|R(x, y) - R_c| \leq \sqrt{2c}$. To guarantee that after jumps from $\mathcal{D}_2$ the state z belongs to $\mathcal{C}_1$, we design the parameters c and d to satisfy

$$d > \sqrt{2c} \tag{78}$$

This is the relationship between c and d given in Eq. (78). With these choices, we have

$$\mathcal{D}_2 \subset \mathcal{C}_1.$$

Additionally, c is chosen such that

$$\mathcal{C}_2 \cap \{z \in U \ : \ R = R_C\} = \emptyset$$

so as to avoid reaching the singularity of Ψ_{C2} given in Eq. (34), which is used in the global controller given in Eq. (59) for points along the loiter circle. This requirement leads to the additional constraint on c given by

$$c > \frac{1}{2}\left(\pi^2 + (v_{\max} - v_{\min})^2\right) \tag{79}$$

Now, according to Proposition 4, from points in $\mathcal{C}_1$ we have that solutions are such that the error e_1 satisfies [7]

$$V_1(e_1(t)) \leq \exp(-\bar{\alpha}(t - t_0'))V_1(e_1(t_0')) + (1 - \exp(-\bar{\alpha}(t - t_0')))\epsilon$$

over each interval of flow (starting at some time t_0') with $q = 1$, where $\bar{\alpha} = 2\min\left\{\frac{v_{\min}\beta R_C}{(R_C^2+(R_C+d)^2)}, \frac{k_{T_1}}{m}, \chi\right\}$. Hence, for each such solutions, $t \mapsto e_1(t)$ is such that $t \mapsto V_1(e_1(t)) = \frac{1}{2}|e_1(t)|^2$ converges to $[0, \epsilon]$, and we have that

$$\lim_{t\to\infty} |e_1(t)| \leq \sqrt{2\epsilon}$$

as long as the solution stays in $\mathcal{C}_1$. To ensure the latter property, we pick

$$\sqrt{2\epsilon} < d$$

which guarantees that $|e_1(t)| \leq \sqrt{2\epsilon}$ for all t in the domain of e_1, which, in particular, implies that $|R(x(t), y(t)) - R_c| < d$ for each such t. Hence, the solutions remain in $\mathcal{C}_1$.

When the parameters c and d are chosen as above, the closed-loop system in Eq. (16) with data as in Eqs. (17)-(20), where κ_1 is given as in (68) and κ_2 as in (59) has the following properties:

- For every point in $\mathcal{C}_2$, solutions with $q = 2$ approach $\mathcal{D}_2$, converge to it in finite time, and a switch to the local controller ($q = 1$) occurs.
- For every point in $\mathcal{C}_1$, solutions with $q = 1$ stay in $\mathcal{C}_1$ and the error quantity $t \mapsto |e_1(t)|$ approaches the set $[0, \sqrt{2\epsilon}]$.
- For every point in $\mathcal{D}_q$, a jump that toggles q occurs.

These properties are validated numerically in the next section.

Although the design of the individual controllers and the supervisory algorithm leading to the closed-loop system in Eq. (16) with data as in Eqs. (17)-(20) is done in nominal, disturbance-free conditions, the design guarantees certain

[7] With some abuse of notation, solutions are parameterized by t only.

robustness to disturbances. Certainly, persistent disturbances such as unmodeled dynamics and measurement noise will prevent trajectories from converging to the set $\mathcal{A}$ in (21). When the norm of those disturbances is small, trajectories from compact sets are expected to converge to points that are nearby the nominal set $\mathcal{A}$ in (21) – this property can be formalized by redefining the flow and jump sets as closed sets, which would necessarily lead to a smaller basin of attraction, and applying the results in [6]. Furthermore, due to the use of hysteresis in the switching mechanism, the proposed controller does not suffer from chattering along the boundary of the jump set as long as the disturbances are small enough, which can be quantified as a function of the constants c and d in the proposed controller. Due to the properties of the Lyapunov-like functions in Propositions 1-4, the tools in [19] for the study of input-to-state stability and in [20] for the robust design of controllers using control Lyapunov functions can be used to precisely characterize the effect of large disturbances in the closed-loop system.

4. Numerical Analysis

The hybrid system for the UAV transition between transit and loiter was implemented in the Hybrid Equations (HyEQ) Toolbox [21] to further explore and verify the analytical results presented. Note that the fact that the flow set $\mathcal{C}$ and $\mathcal{D}$ overlap requires imposing a desired semantics when flows are possible from such overlaps. For instance, a trajectory that reaches a point in the boundary of $\mathcal{C}_2$ that is also in $\mathcal{D}_2$, could experience a jump, in which case the value of q for that trajectory will become equal to 1, or potentially flow for some time along the common boundary of those two sets. While either behavior is appropriate, since the choice of the constants in Section 3.3 guarantee that all trajectories approach the target set $\mathcal{A}$, the simulations are performed using *forcing semantics*: whenever a trajectory reaches the jump set, a jump is executed.

Table 1: Simulation Parameters

UAV	Value	Units	Scenario	Value	Units	Gain	Value
W	24525	N	μ	0.1	-	ξ	see Eq. (80)
C_{Lmax}	0.85	-	v_{C_1}	160	$\frac{m}{s}$	k_{T_1}	1000
C_{D0}	0.002	-	v_{C_2}	200	$\frac{m}{s}$	k_{T_2}	1000
K	59	-	ρ	1.112	$\frac{kg}{m^3}$	ζ	0.1745
S_{ref}	35.15	m^2	g	9.81	$\frac{m}{s^2}$	γ	see Eq. (81)
T	[50 9000]	N				χ	10
						ν	10

The inputs and gains used for the presented simulation results are listed below in Table 1. Several of the gain parameters listed in the table vary as a function of the vehicle's flight conditions while still satisfying the constraints

established in the control law analysis. The criteria for varying the gains is listed below.

$$\xi = \frac{3}{2\pi}|\Delta_2|. \tag{80}$$

$$\gamma = \frac{3}{2\pi}|\Delta_1|. \tag{81}$$

The local/global switching criteria for the simulation were set as

$$c = \frac{1}{2}(\pi^2 + (v_{\max} - v_{\min})^2) + 1 \tag{82}$$

$$d = \sqrt{2c} + 200 \tag{83}$$

where Eq. (82) and Eq. (83) were selected to satisfy Eq. (79) and Eq. (78) respectively. Simulation results are shown to demonstrate the performance of the algorithm.

4.1. Outside the Loiter Circle (Disk)

For the scenario starting outside the loiter circle a loiter radius (R_C) of 350 m was used. Figure 8 shows a performance time history for the trajectory. The vehicle is initially headed in the wrong direction, but the global controller reverses heading to fly towards the center of the loiter circle. The hysteresis between $\mathcal{C}_1$ and $\mathcal{C}_2$ prevents chatter between the local and global controllers. The vehicle switches from the global controller to the local controller at a point inside the local controller flow set and follows a trajectory that approaches the loiter circle on a tangent and ultimately tracks the loiter circle. The switch

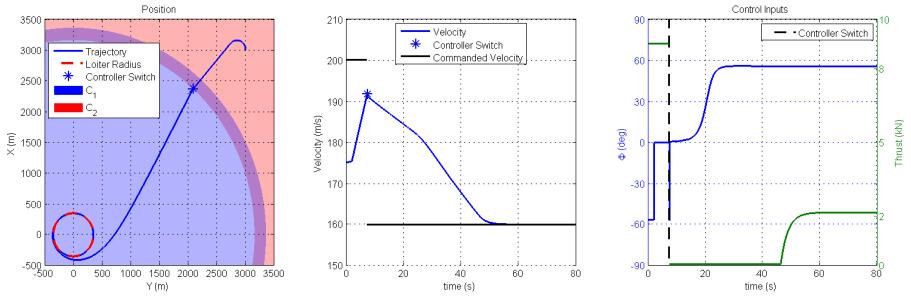

Figure 8: Simulation results starting outside the loiter circle.

from the global controller to the local controller occurs at approximately 7 seconds. In the global control region, the vehicle attempts to accelerate to the commanded global controller velocity. For the first two seconds the vehicle does not accelerate quickly because of the high drag while turning. Once the vehicle has completed its turn it accelerates more quickly to the global commanded velocity until the switch to the local controller. In the local control region, the

thrust is commanded to its minimum while the vehicle decelerates to the commanded loiter velocity.

4.2. Inside the Loiter Circle (Disk)

Figure 9 shows a performance time history for a trajectory starting in the local controller set inside the loiter circle with radius (R_C) of 2500 m. As shown in the position graph, the local controller set $\mathcal{C}_1$ is shaped like a disk because $c > R_C$. The vehicle stays in $\mathcal{C}_1$ indefinitely and no controller switching occurs as the position converges to the loiter circle and the velocity converges to the commanded loiter velocity. The vehicle starts at the center of the loiter circle

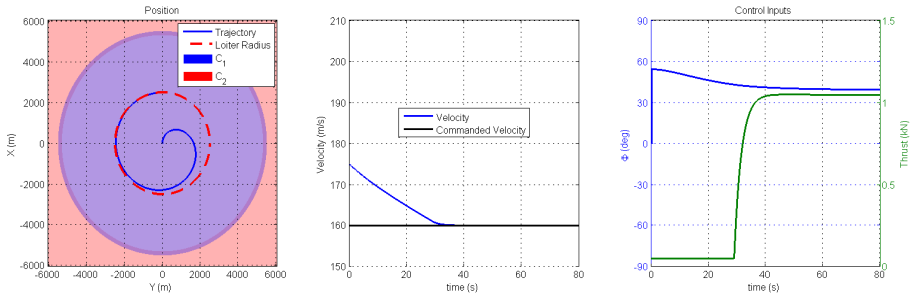

Figure 9: Simulation results starting inside the loiter circle with disk shaped local controller set

and gradually spirals outward for a tangential approach which is constrained by the vehicle's turn radius. The vehicle started out initially faster than the desired loiter velocity and commands the minimum thrust until approximately 7 seconds at which point the thrust gradually approaches the drag as intended by the control law given in Eq.(32).

4.3. Inside the Loiter Circle (Donut)

To demonstrate a scenario with a donut shaped local controller set $\mathcal{C}_1$, a loiter circle with radius (R_C) of 5000 m was used. Figure 10 shows a performance time history for a trajectory starting in the global controller set $\mathcal{C}_2$ inside the loiter circle. At the beginning of the trajectory the vehicle accelerates in a straight line towards the loiter circle. At 12 seconds into the trajectory the vehicle has nearly reached the commanded transit velocity when it enters the local controller set $\mathcal{C}_1$ and the commanded velocity switches. Since the vehicle needs to decelerate to reach the commanded loiter velocity the minimum thrust is commanded. Upon reaching $\mathcal{C}_1$ the vehicle begins banking to maneuver onto the loiter circle trajectory.

The simulation results confirm that the controller design provides the desired performance within each of the local and global modes. Also, the design of the local and global sets prevents chattering between the two modes.

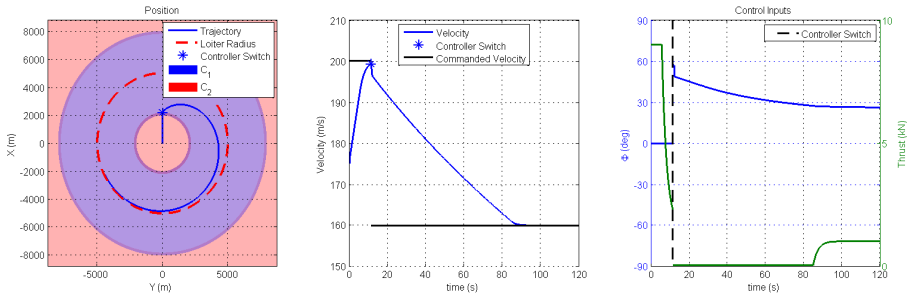

Figure 10: Simulation results starting inside the loiter circle with donut shaped local controller set

5. Conclusion

A hybrid control system for UAV waypoint loitering was analyzed and demonstrated. Asymptotic stability was established, and verified by simulation, for the UAV system modeled in a plane with thrust and bank angle as control inputs. There are several opportunities for future work. One could be to expand the control algorithm to be three dimensions by including altitude and account for time varying mass. Another possibility could be to expand the algorithm to use other modes such as changing altitude. Though this paper focused on a UAV as the system being controlled, the algorithm could be applied to other systems such as boats or wheeled vehicles.

6. Acknowledgment

The first author would like to thank his family for patiently giving up evenings and weekends to let work on this project. Research by R. G. Sanfelice was partially supported by NSF Grants no. ECS-1150306 and CNS-1544396, and by AFOSR Grants no. FA9550-12-1-0366 and FA9550-16-1-0015.

7. References

[1] E. W. Frew, D. A. Lawrence, C. Dixon, J. Elston, and W. J. Pisano. Lyapunov guidance vector fields for unmanned aircraft applications. In *2007 American Control Conference*, pages 371–376, July 2007.

[2] D. Lawrence, E. Frew, and W. Pisano. Lyapunov vector fields for autonomous unmanned flight control. *Journal of Guidance, Control, and Dynamics*, 31(5):1220–1229, 2008.

[3] S. Park, J. Deyst, and J. How. A new nonlinear guidance logic for trajectory tracking. In *AIAA Guidance, Navigation, and Control Conference and Exhibit*, Providence, Rhode Island, 2004.

[4] C. Prieur. Uniting local and global controllers with robustness to vanishing noise. *Math. Control Signals Systems*, 14:143–172, 2001.

[5] V. Parra-Vega and G. Hirzinger. Chattering-free sliding mode control for a class of nonlinear mechanical systems. *International Journal of Robust and Nonlinear Control*, 11(12):1161–1178, 2001.

[6] R. Goebel, R. G. Sanfelice, and A. R. Teel. *Hybrid Dynamical Systems: Modeling, Stability, and Robustness*. Princeton University Press, 2012.

[7] C. Prieur, R. Goebel, and A. R. Teel. Hybrid feedback control and robust stabilization of nonlinear systems. *IEEE Transactions on Automatic Control*, 52(11):2103–2117, November 2007.

[8] R. G. Sanfelice, A. R. Teel, and R. Goebel. Supervising a family of hybrid controllers for robust global asymptotic stabilization. In *Proc. 47th IEEE Conference on Decision and Control*, pages 4700–4705, Cancun, Mexico, 2008.

[9] R. G. Sanfelice and A. R. Teel. A "throw-and-catch" hybrid control strategy for robust global stabilization of nonlinear systems. In *Proc. 26th American Control Conference*, pages 3470–3475, New York, NY, 2007.

[10] D. Efimov, A. Loria A., and E. Panteley. Robust output stabilization: Improving performance via supervisory control. *International Journal of Robust and Nonlinear Control*, 21(10):1219–1236, 2011.

[11] B. M. Chen A. Karimoddini, H. Lin and T. H. Lee. Developments in hybrid modeling and control of unmanned aerial vehicles. In *Proc. 2009 IEEE International Conference on Control and Automation*, pages 228–233, Christchurch, New Zealand, 2009.

[12] E. Frazzoli, M. A. Dahleh, and E. Feron. Maneuver-based motion planning for nonlinear systems with symmetries. *Robotics, IEEE Transactions on [see also Robotics and Automation, IEEE Transactions on]*, 21:1077–1091, 2005.

[13] R. G. Sanfelice and E. Frazzoli. A hybrid control framework for robust maneuver-based motion planning. In *Proc. 27th American Control Conference*, pages 2254–2259, 2008.

[14] D. Jung and P. Tsiotras. Bank-to-turn control for a small uav using backstepping and parameter adaptation. *Proceedings of 17th IFAC World Congress*, 17(1):4406–4411, 2008.

[15] A. Witkowska and R. Smierzchalski. Nonlinear backstepping ship course controller. *International Journal of Automation and Computing*, 2009.

[16] M. Krstic, I. Kanellakopoulos, and P. Kokotovic. *Nonlinear and Adaptive Control Design*. Wiley-Interscience, New York, 3rd edition, 1995.

[17] H. Khalil. *Nonlinear Systems*. Prentice Hall, 3rd edition, 2002.

[18] D. Raymer. *Aircraft Design: A Conceptual Approach*. American Institute of Aeronautics and Astronautics Inc., 4th edition, 2006.

[19] C. Cai and A. R. Teel. Characterizations of input-to-state stability for hybrid systems. *Syst. & Cont. Letters*, 58:47–53, 2009.

[20] R. G. Sanfelice. Robust asymptotic stabilization of hybrid systems using control lyapunov functions. In *Proceedings of the 19th International Conference on Hybrid Systems: Computation and Control*, pages 235–244, April 2016.

[21] R. G. Sanfelice, D. A. Copp, and P. Nanez. A Toolbox for Simulation of Hybrid Systems in Matlab/Simulink: Hybrid Equations (HyEQ) Toolbox, Proceedings of Hybrid Systems: Computation and Control Conference, August 2013.